Special Collection

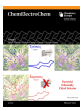

Trópos and *Átropos* Biindole Chiral Electroactive Monomers: A Voltammetry and HPLC Comparative Insight

Serena Arnaboldi,[a] Sara Grecchi,[a] Luca Vaghi,[b] Andrea Penoni,[c] Luca Scapinello,[c] Ivo Franco Buzzi,[a] Roberto Cirilli,[d] Marco Pierini,*[e] Tiziana Benincori,*[c] and Patrizia Romana Mussini*[a]

A series of 2,2′-biindole-based inherently chiral electroactive monomers are comparatively investigated with their 3,3′ analogues as an excellent study case of two equivalent redox centres interacting through a torsional barrier. The twin peak potential splitting observed in voltammetry for the first oxidation of the biheteroaromatic core accounts for the energy barrier height: the lower the barrier, the larger the peak potential splitting, with modulation by solvent and temperature. The height of the energy barrier is determining for the electrochemical and spectroscopic features of the monomers as well as for their configurational stability and applicability for enantioselection purposes. The 3,3′ monomers, featuring large twin peak splittings in CV, are "trópos" systems with a low torsional barrier, so they cannot exist as stable enantiomers at room temperature. Instead their 2,2′ isomers, with much smaller twin peak splittings, are "átropos" systems and can be separated by enantioselective HPLC into stable enantiomers, providing powerful "inherently chiral" selectors with outstanding enantioselection properties in chiral electroanalysis and electrochemistry as well as in chiroptical spectroscopy, with fascinating reciprocal correlations.

Introduction

A winning strategy to achieve chiral electrode surfaces of huge and wide-scope enantiodiscrimination ability consists in the electrodeposition of "inherently chiral" oligomer films from electroactive monomers[1] of helical or axial stereogenicity, *i.e.* based either on a helical backbone[2] or on an atropisomeric one, that is, consisting of two, usually identical, moieties with reciprocal high sterical hindrance.[3–8] In such monomers, both chirality and key functional properties, like electrochemical and optical activity, originate from the whole main molecular backbone, featuring a tailored torsion associated with an energy barrier (enantiomerization barrier) too high to be overcome at room temperature.[1] Thus such molecules can exist as stable (*R*)- and (*S*)-enantiomers, that can be separated and stored; they also fully retain their configuration when electro-oligomerizing, yielding (*R*)- or (*S*)-enantiopure oligomer films.[3] Such electrode surfaces result in significant, often wide, potential differences for the enantiomers of a variety of chiral electroactive probes in voltammetry experiments,[3–10] which can be ascribed to energetically different conditions for the probe enantiomers at the enantiopure surface, achieved through the many coordination elements available (heteroatoms and π conjugated systems).[11–14] The axial stereogenicity approach, combining high three-dimensional character and oligomerization ability with convenient synthesis and wide structure modulability, has been so far more exploited than the helical one. In particular, it has been so far implemented exploiting monomers based on four atropisomeric biheteroaromatic cores, *i.e.* 3,3′-bibenzothiophene,[3,9,10] 3,3′-bithiophene,[4] 2,2′-biindole[5–7] and 1,1′-binaphthyl[8] ones, in all cases combined with symmetrical oligothiophene-based terminals (some examples are reported in Figure 1). Besides their above highly successful application for chiral electroanalysis, such monomers are also attractive model systems in the frame of intramolecular charge communication studies.

Communication between equivalent redox centres in electroactive molecules is a fundamental and fascinating subject.[15–18] It is of course first of all a function of the nature of the linker between them, *i.e.* double bond(s), triple bond(s),

[a] *Dr. S. Arnaboldi, S. Grecchi, I. F. Buzzi, Prof. P. R. Mussini*
Dipartimento di Chimica
Università degli Studi di Milano
Via Golgi 19, 20133 Milano, Italy
E-mail: patrizia.mussini@unimi.it
[b] *Dr. L. Vaghi*
Dipartimento di Scienza dei Materiali
Università degli Studi di Milano-Bicocca
Via Cozzi 55, 20125 Milano, Italy
[c] *Prof. A. Penoni, Dr. L. Scapinello, Prof. T. Benincori*
Dipartimento di Scienza e Alta Tecnologia
Università degli Studi dell'Insubria
Via Valleggio 11, 22100 Como, Italy
E-mail: tiziana.benincori@uninsubria.it
[d] *Dr. R. Cirilli*
Centro Nazionale per il Controllo e la Valutazione dei Farmaci
Istituto Superiore di Sanita'
Viale Regina Elena 299, 00161 Roma, Italy
[e] *Prof. M. Pierini*
Dipartimento di Chimica e Tecnologie del Farmaco
Università degli Studi di Roma "La Sapienza"
Piazzale Aldo Moro 5, 00185 Roma, Italy
E-mail: marco.pierini@uniroma1.it

Supporting information for this article is available on the WWW under https://doi.org/10.1002/celc.202100903

An invited contribution to a joint Special Collection in memory of Prof. Jean-Michel Savéant

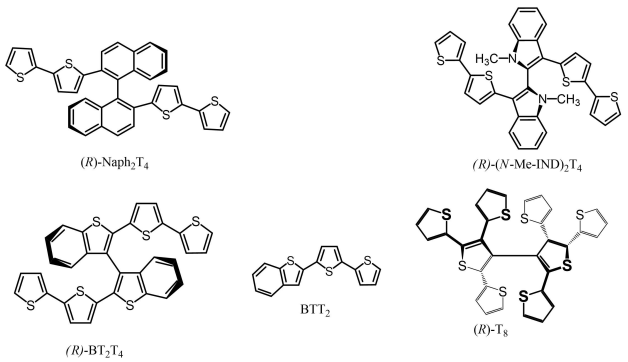

Figure 1. Examples of electroactive monomers with axial stereogenicity originating from atropisomeric bi(hetero)aromatic cores. For our parent studycase BT_2T_4 molecule, the BTT_2 achiral moiety is also reported.

(hetero)aromatic ring(s), aliphatic chain… or none (redox centres directly linked), as highlighted in many studies (like *e.g.*[15–29]).

Furthermore, communication can also take place in 3D space rather than along a conjugated system.[23,29,30,31] The medium has an important role, too, in terms of charge screening and/or of promoting aggregation *vs* distancing of the redox sites.[17,18,31]

In this context, it is important to realize that a powerful role on the extent of reciprocal communication between redox centres can also be played by conformational issues,[32] a topic so far less explored, such as, for example, a torsion possibly present in the molecular backbone.

Biheteroaromatic atropisomeric monomers provide a fascinating model case, consisting of two identical redox sites with no interposed linker, but with a torsional energy barrier depending on the biheteroaromatic core structure. Notably, such barrier is at the same time determining for:

(*i*) *the configurational stability of the monomer*. In fact, around a threshold value of about 25 kcal/mol (that is, about 104 kJ/mol), racemization can increasingly take place at room temperature, and the monomers should be considered "*trópos*" systems (from Greek *trepein*, *i.e.* to turn around), like *e.g.* unsubstituted biphenyl, rather than "*átropos*" ones; importantly, only "*átropos*" monomers can be exploited as stable enantiopure selectors;

(*ii*) *the backbone overall conjugation efficiency*, which increases with decreasing energy barrier, thus affecting both optical and electrochemical properties; in particular increasing overall conjugation results in higher absorption wavelength as well as in less extreme first oxidation and first reduction potentials, and in narrower HOMO-LUMO gaps;

(*iii*) *loss of energy level degeneration*, on account of significant interaction between the two molecule moieties, representing at the same time two equivalent chromophores as well as two equivalent redox centres; this effect results in typical chiroptical and electrochemical fingerprints.

In particular, in spectroscopy interaction between equivalent chromophores results in a difference in their excited energy levels, and therefore in their absorption wavelengths; such difference is however unconspicuous in the UV-vis spectrum since the sum of the two adjacent absorption peaks results in a single wider one, but can be well evidenced for inherently chiral molecules by recording in the same wavelength range their circular dichroism spectrum. In fact, in that case their absorption peaks are reciprocally subtracted, resulting in a typically sigmoidal signature, specular for (*R*)- and (*S*)-enantiomers ("Davydov splitting"), modulated by the relative angle between interacting chromophore dipole moments in space, with a maximum at nearly 90°.[33,34]

At the same time, in electrochemistry, the two interacting equivalent redox centres result in twin peak systems in voltammetry experiments, with a potential difference increasing with increasing reciprocal interaction, implying increasing conjugation efficiency[15] (actually even two non-interacting equivalent redox centres have, when belonging to the same molecule, a very small standard potential difference, of about 35 mV, on account of the so called "entropic effect"; however, their CV pattern is a single peak of double height and half-peak width consistent with a monoelectronic process[15]). Such potential difference can also be exploited to classify such systems according to the extent of communication (assuming the electronic interaction to be the predominant one in the present case; in some cases other interactions can also take place between redox centres, as discussed in[16]), as Type I, II, or III according to the Robin and Day scheme, depending on $K_c = \exp(F\Delta E_{1/2}/RT)$, with $E_{1/2}$ = half wave potential (which can be assumed to coincide with formal potential $E^{\circ\prime}$) for the two electron transfer processes, and K_c = comproportionation constant for the equilibrium $[M^{n+1}-M^{n+1}][M^{n}-M^{n}] \rightleftarrows 2[M^{n+1}-M^{n}]$.[21,26,28,32]

Attractively, considering the above connections between the torsional barrier implications on the monomer functional properties, the observed loss of degeneration in the voltammetric pattern should provide clues not only about the extent of the electronic communication between redox centres, but also about the activation energy value that opposes to the enantiomerization process, and thus the configurational stability, *i.e. átropos vs trópos* nature of the monomer.

As a convenient model case, to our knowledge a proof-of-concept one from the electrochemical perspective, the voltammetric features will be compared of two series of biindole-based atropisomeric monomers, **1a**, **2a**, **2b** and **3**, **4a**, **4b**, constituted by identical building blocks but

(*i*) different connectivity between biindole core moieties, *i.e.* 2,2′[5,6] *vs* 3,3′ (with wings conversely attached in 3,3′ and in 2,2′ positions respectively, Figure 2), a feature which we realized has a huge impact on the potential difference for the twin peak system;

(*ii*) and without or with a phenyl spacer[6] between the biindole core and the (bi)thiophene terminals, a feature affecting the core/terminal conjugation.

Monomers **1b** and **4c**, useful for sake of comparison, will also be considered.

Peculiar focus will be on first oxidations, which mostly involve the biindole core moieties and therefore account for their reciprocal communication.

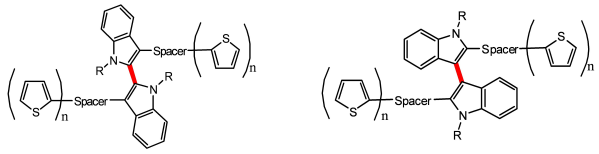

2,2′-biindole core
1a: Spacer = none, n = 2, R = Me
1b: *Spacer= none, n = 2, R = Hex*
2a: Spacer= Ph, n = 2, R = Me
2b: Spacer= Ph, n = 2, R = Hex

3,3′-biindole core
3: Spacer = none, n = 2, R = Me
4a: Spacer= Ph, n = 2, R = Me
4b: Spacer= Ph, n = 2, R = Hex
4c: *Spacer= Ph, n = 1, R = Hex*

Figure 2. A molecular structure synopsis of the electroactive biindole-based monomers discussed in this paper

The discussion of the electrochemical features will be complemented with enantioselective HPLC, chiroptical and computational results, accounting for the monomer enantiomerization barriers, to highlight the connections between voltammetric fingerprints and *átropos* or *trópos* nature, and thus configurational stability as enantiopure antipodes, of the model monomers.

Results and Discussion

Synthesis of 2,2′- and 3,3′-Biindole Derivatives

The 2,2′-biindole based compounds **1a**,[5] **1b** and **2a,b**[6] were synthesized following the Larock[35,36] protocol developed by Abbiati[37] in which the formation of the 2,2′-biindole core and its functionalization in 3 and 3′-positions take place in one step, although in modest yield. The key intermediate is the butadiine derivative **5**[38,39] that was made to react with the suitable haloderivative, namely the 5-iodo-2,2′-bithiophene and the 5-(4-bromophenyl)-2,2′-bithiophene,[40] in the presence of $Pd(PPh_3)_4$ as catalyst and K_2CO_3 as a base. Finally, in order to confer configurational stability, the intermediates **6** and **7** were functionalized at the nitrogen atoms with the suitable alkyl groups by reaction of the corresponding bis-anions, generated with KOH in DMF (Scheme 1).

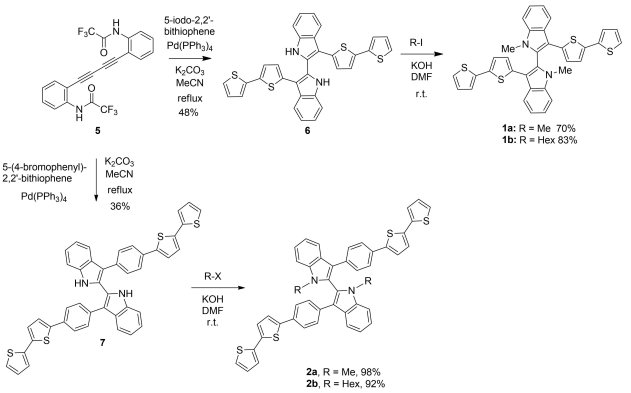

Scheme 1. Synthesis of 2,2′-biindole derivatives **1a,b** and **2a,b**.

The synthesis of the 3,3′-biindole **3** was carried out through a Brønsted acid catalyzed reaction of the 2-[(aminophenyl)ethynyl]phenylamine **8**[41] with the 2,2′-bithiophene-5-carboxy-aldehyde[42] developed by Arcadi mainly with aryl aldehydes.[43] The crude of the reaction, containing the intermediate **9**, was made to react with KOH and MeI; biindole **3** was isolated in 29% yield, after a careful column chromatography (Scheme 2).

The synthesis of the 3,3′-biindoles functionalized in the 2,2′ positions with phenyl(bi)thienylic wings was performed starting from the dibromoderivative **10** obtained, according to the literature, through the homo-coupling of 2-(4-bromophenyl)-indole by the use of $FeCl_3$ as catalyst and molecular oxygen as oxidant .[44] After alkylation of the indole units with the suitable halocompounds, the dibromoderivatives **11a** and **11b** were converted into the final compounds **4a–c** through a tetrakis (triphenylphosphine) palladium(0) catalyzed Suzuki coupling with the commercially available 2-(2,2′-bithien-5-yl)-4,4,5,5-tetramethyl-1,3,2-dioxaborolane and 2-thienylboronic acid, respectively (Scheme 3).

Communication between Bisindole Core Moieties in 2,2′- and 3,3′-Biindole Derivatives Investigated by Cyclic Voltammetry in Low-Polarity Solvent Dichloromethane

To discuss the electronic communication between the biindole core moieties with little medium screening effect it is convenient to consider cyclic voltammetry (CV) patterns recorded for the monomers in a low-polarity solvent such as dichloromethane.

It is also useful to start by briefly recalling as a reference the features of the prototype bibenzothiophene-based case BT_2T_4[3] consisting of two BTT_2 (Figure 1) equal moieties, each one including a benzothiophene decorated in α position with a 2,2′-

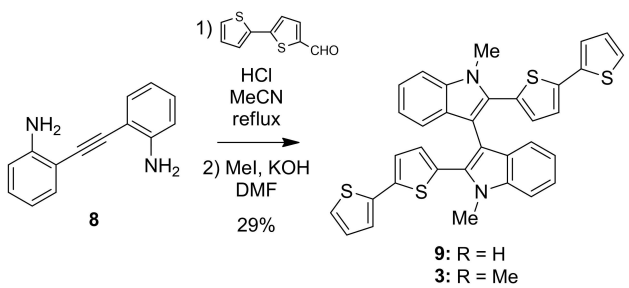

Scheme 2. Synthesis of 3,3′-biindoles **9** and **3**.

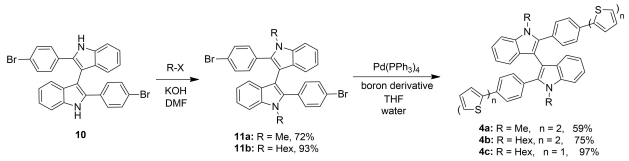

Scheme 3. Synthesis of 3,3′-bisindole derivatives **4a–4c**.

bithiophene, and therefore featuring an α-terthiophene system (Figure 1).

The first oxidation CV features of BT_2T_4 consist in a nearly merging ($\Delta E_p \sim 0.08$ V at 0.2 V/s) twin system of peaks chemically irreversible at low scan rates but increasingly reversible at higher ones. This system is located close to the single first oxidation peak observed for a single monomer moiety BTT_2 ([3] with related SI), in a potential range close to first oxidation of α-terthiophene[45] (normalized *vs* $Fc^+|Fc$[46]). Both such nearly merging twin peak pattern and the terthiophene-like reactivity are consistent with only moderate communication existing between the two monomer moieties, which is in turn consistent with the calculated very high torsional barrier (about 40 kcal/mol) and torsional angle (about 80°) of BT_2T_4.[3] Importantly, each first oxidation site is delocalized on the whole terthiophene system in each BTT_2 moiety, which is not only consistent with the oxidation potential, but also confirmed by the observation that monomer oligomerization (based on radical cation coupling in α-thiophene terminal positions) takes place by cycling the potential just around the first oxidation peak twin system ([3] with related SI). The very high energy barrier also results in high stability of the enantiomers, which can be efficiently separated by enantioselective HPLC.[3,47] On the spectroscopy side, the circular dichroism spectrum of BT_2T_4 shows a neat Davydov splitting with maxima/minima at about 360 and 410 nm, accounting for a remarkable loss of degeneration for the absorption wavelengths of the two equal chromophores corresponding to the molecule moieties as a consequence of their interaction in space, although the corresponding UV-Vis spectrum only features a unique large absorption peak ([3] with related SI).

Changing the 3,3′-bibenzothiophene core with a 2,2′-biindole one (at constant bithiophene terminals), *i.e.* considering monomer **1 a**, the equivalent first oxidation sites on the two molecule moieties still involve the core heterocycles conjugated to the bithiophene terminals, but are mostly centered on the pyrrole rings in the molecule core, being significantly more electron rich than thiophene ones.[5] As a consequence, a system of twin chemically reversible first oxidation peaks is observed, since the radical cations resulting from the electron transfers are mostly localized on the core, far away from the thiophene terminals. This is confirmed by oligomerization being only achieved by cycling around a further peak system, corresponding to second oxidations located on the thiophene terminals.[5] Importantly, the reciprocal distance in the first twin peak system is much larger than in the BT_2T_4 case[5] (Figure 3, Table 1), ($\Delta E_p \sim 0.2$ V at 0.2 V/s), which is consistent with the much lower energy barrier of **1 a** (27–30 kcal/mol[5]) with respect to BT_2T_4, which is however still sufficiently high to have stable enantiomers at room temperature, obtained *e.g.* by enantioselective HPLC.[5] The CD spectrum again features a remarkable Davydov splitting (depending on the chromophore dipole angle in space), comparable to the BT_2T_4 one, with maxima/minima at about 340 and 380 nm.[5]

Changing the length of the alkyl substituents at N atoms from methyl to hexyl ones (monomer **1 b**) has only little effects on the first oxidation features, including a small shift to more positive potentials as well as some increase in the twin peak distance (Figure 3, Table 1), while the electrooligomerization ability (upon cycling around the further oxidation peak, appearing as a single one at 0.2 V/s but tending to slightly split at higher scan rates) significantly decreases, in line with the higher solubility promoted by longer alkyl chains.

A phenyl group inserted between core and terminals (monomers **2 a**, **2 b**) acts more as a spacer than as a linker,[6] resulting in a first oxidation twin peak system localized on the biindole core and shifted at significantly more positive potentials, since no more benefit can come from conjugation with adjacent thiophene rings (Figure 3, Table 1,[6]). A further oxidation system localized on the bithiophene terminal follows, at a potential close to α-bithiophene oxidation ([45] normalized *vs* $Fc^+|Fc$[46]). (Figure 3, Table 1,[6]). In other words, the phenyl spacer makes core and terminal oxidations nearly independent. Remarkably, it also results in significantly closer twin peaks for the biindole core oxidation ($\Delta E_p \sim 0.1$ V at 0.2 V/s), pointing to a conformation implying lower interactions between the two moieties, which looks consistent with the phenyl ring enhancing the sterical hindrance effect between the two core moieties in the 2,2′-bisindole series (Figure 3, Table 1,[5]). Instead, as above mentioned, increasing the length of the aliphatic chain substituents on the N atoms results in some increase of the CV twin peak distance. This intriguing feature will be further discussed in connection with the theoretical computation results.

From the chiroptics point of view, the antipodes of monomers **2 a** and **2 b** also feature neat Davydov splittings in their CD spectra[6] like parent **1 a**.[5]

Although when comparing BT_2T_4 with 2,2′-biindoles (especially **1 a** having the same bithienyl terminals with no spacer and the shorter alkyl substituent) the implications emerge of the enantiomerization energy barrier on voltammetric fingerprints, in order to perform a sound investigation specifically

Table 1. Key features of the monomer CV patterns in CH_2Cl_2 at 0.2 V/s. Potentials are expressed in volts and referred to $Fc^+|Fc$.

	E_{pI}	$E^{o\prime}{}_I$	E_{pII}	$E^{o\prime}{}_{II}$	E_{pII}-E_{pI}	$E^{o\prime}{}_I$-$E^{o\prime}{}_{II}$	E_{III}
2,2′-(N–Me)Ind_2T_4 (**1 a**)	0.38	0.33	0.55	0.51	0.17	0.18	0.80,0.92
3,3′-(N–Me)Ind_2T_4 (**3**)	0.25	0.22	0.57	0.54	0.32	0.32	1.12
2,2′-(N-Hex)Ind_2T_4 (**1 b**)	0.39	0.36	0.62	0.59	0.23	0.23	0.82, 1,08
2,2′-(N–Me)$Ind_2Ph_2T_4$ (**2 a**)	0.57	0.52	0.69		0.12		0.88
3,3′-(N–Me)$Ind_2Ph_2T_4$ (**4 a**)	0.23	0.19	0.57	0.55	0.34	0.36	0.86
2,2′-(N-Hex)$Ind_2Ph_2T_4$ (**2 b**)	0.49	0.43	0.62		0.13		0.80
3,3′-(N-Hex)$Ind_2Ph_2T_4$ (**4 b**)	0.21	0.20	0.63	0.62	0.42	0.42	0.75,1.04
3,3′-(N-Hex)$Ind_2Ph_2T_2$ (**4 c**)	0.20	0.17	0.62	0.59	0.42	0.42	1.31

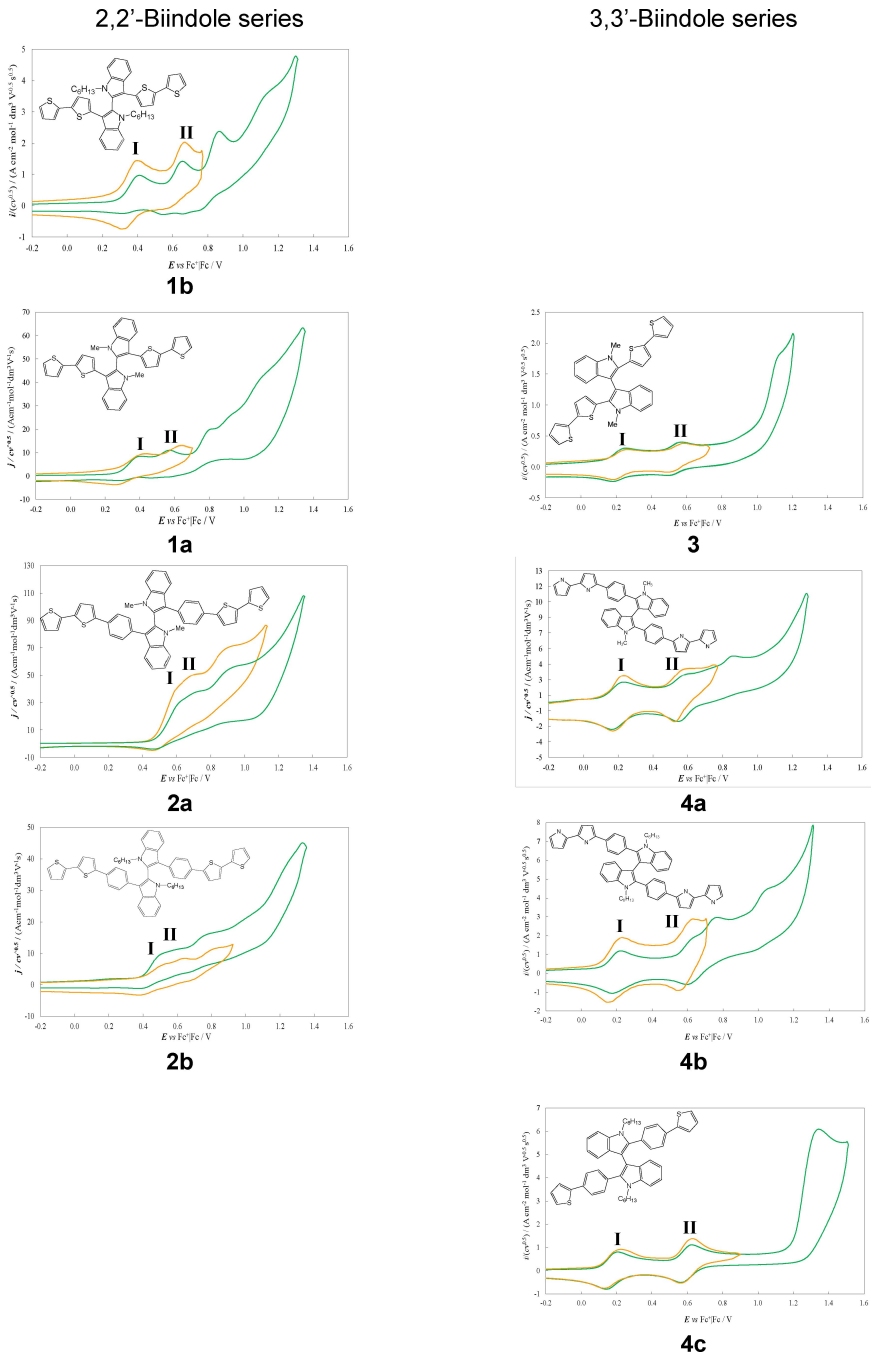

Figure 3. A synopsis of the normalized 2,2′ (left) and 3,3′ (right) monomer CV patterns in CH_2Cl_2 at 0.2 V/s (or 2 V/s, superimposed orange pattern). Side by side are 2,2′ and 3,3′ analogue pairs.

focused on this topic, model systems should be considered consisting of identical chemical building blocks but different connectivity resulting in different energy barriers. Moreover, the study should include cases with energy barriers below the "security zone" for enantiomer stability, *i.e.* lower than the above mentioned ~25 kcal/mol energy threshold corresponding to transition from *átropos* to *trópos* systems. A very good option is provided by 3,3′-biindole monomers **3**, **4a** and **4b**, to be directly compared to their analogues **1a**, **2a** and **2b** in the 2,2′-biindole monomer series. Their oxidative CV patterns are reported in Figure 3 to the right of the corresponding 2,2′-analogues, and the relevant potentials in Table 1. The Figure also includes monomer **4c**, differing from **4b** for having thiophene rather than bithiophene terminals beyond the phenyl spacers, and for this reason providing a very good benchmark in the CV discussion.

In fact the irreversible oxidation of the terminals is in this case shifted to a much more positive potential, consistent with simple thiophene oxidation ([45] normalized *vs* $Fc^+|Fc$[46]) which once more confirms the phenyl group to act more than a

spacer than a linker, and the biindole core oxidation is very well showcased as a twin system of canonically reversible peaks at a very large distance (both peak potential difference, $\Delta E_p = E_{pII} - E_{pI}$, and formal potential difference, $\Delta E^{\circ\prime} = E^{\circ\prime}_{pII} - E^{\circ\prime}_{pI}$, are ~0.42 V) and with the first peak at a potential remarkably less positive with respect to the 2,2′ cases. These two features point to a remarkably lower torsional energy barrier between the two moieties, resulting in much higher conjugation efficiency and very strong interaction between the two indole redox sites.

Monomer **4b**, only differing from **4c** for having bithiophene terminals, features practically the same biindole oxidation pattern, with the bithiophene terminal oxidation starting quite close at a slightly more positive potential, consistent with that expected for an independent bithiophene ([45] normalized *vs* $Fc^+|Fc$[46]).

Monomer **4a**, having methyl rather than hexyl substituents on the N atoms, shows a smaller $\Delta E^{\circ\prime}$ than **4b**, analogously to the already discussed parallel **1a** *vs* **1b** case in the 2,2′ series. A further analogy is that **4a** gives fast and regular electro-oligomerization by cycling the potential around the terminal oxidation peak, while **4b** does not, possibly on account, again, of the effects of its hexyl chains.

Monomer **3**, also having a methyl substituent but no phenyl spacer, has $\Delta E^{\circ\prime}$ close to **4a** for the biindole system, while the bithiophene terminal oxidation takes place at a considerably higher potential, which could be explained in terms of communication with the biindole site.

On the whole, in spite of some modulation, the whole 3,3′ series has for the biindole core a much larger $\Delta E^{\circ\prime}$ (0.31−0.42 V) than the 2,2′ series (0.07−0.18 V), with a first peak at $E^{\circ\prime}$ = 0.17−0.24 V ($Fc^+|Fc$) with respect to $E^{\circ\prime}$ = 0.33−0.52 V ($Fc^+|Fc$). In terms of Robin Day classifications, the 3,3′ series would belong to class III (strong interactions, complete delocalization) while the 2,2′ one to class II (weak interactions, partial communication).

Thus, clearly, the 3,3′ connectivity must correspond to a much lower torsional barrier, enabling very efficient communication between the two equivalent indole redox centres. This can be confirmed by enantioselective HPLC experiments combined with computational studies.

Experimental and Computational Analysis of the Stereo-stability of 2,2′-Bindole Monomers 1a, 1b, 2a, 2b *vs* 3,3′-Biindole Monomers 3, 4a, 4b and 4c

The tendency of 2,2′-bindole monomers **1a**, **1b**, **2a**, **2b** and of 3,3′-biindole monomers **3**, **4a**–**4c** to retain stable *R* or *S* configurations has been investigated both experimentally and theoretically. The experimental studies were performed by resorting to:

(*i*) *enantioselective Dynamic HPLC* (*D-eHPLC*), for monomers that evidenced appreciable stereolability not far from the room temperature, with enantiomerization barriers characterized by $\Delta G^{\#}$ values below 25 kcal mol^{-1}. This was evident from the appearing of typical plateau regions between the peaks of separated enantiomers, increasingly with increasing temperature (Figure 4). Such curve shapes are quantitatively indicative of a competitive enantiomerization process occurring during the enantioseparation, and through their computer-driven simulation it is possible to assess kinetic and thermodynamic information including related enantiomerization rate constants;[48–58]

(*ii*) *enantioselective HPLC off-column racemization* (*eHPLC*) for monomers with stable configurations at temperature values higher than 25 °C (from 60 to 90 °C), which implies the absence of the above chromatographic-profile deformations. In such cases, optimized enantioselective HPLC protocols were exploited to monitor the enantiomeric

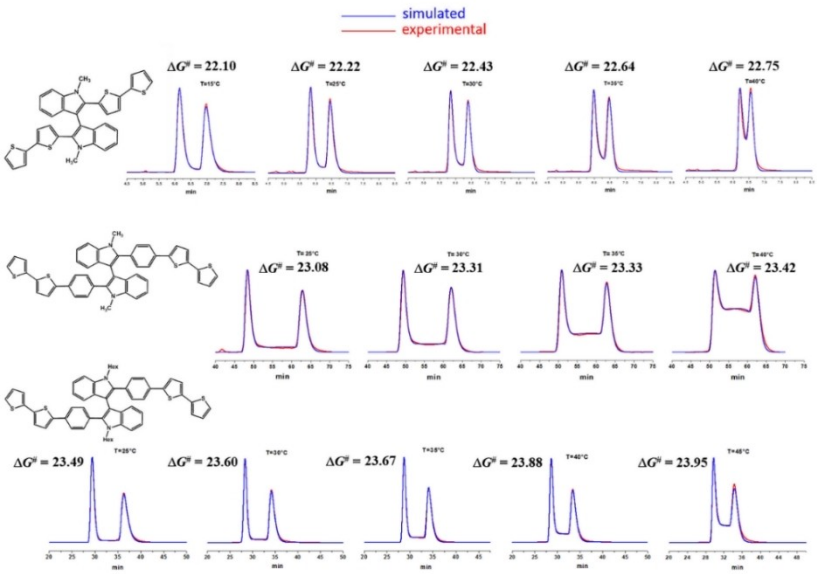

Figure 4. Line shape analysis of the dynamic chromatograms registered for the **3**, **4a** and **4b** 3,3′-biindole derivatives.

excess decay occurring over time outside the chromatographic column.[53,59–63]

Theoretical assessments were also flanked to several of these determinations. This was done through the choice of suitable computational conditions and procedures, not very expensive in terms of calculus times, able to allow a good reproduction of the experimentally found $\Delta G^{\#}$ barriers at the room temperature of 25 °C. In particular, theoretical estimations were conducted following two independent approaches, based:

(*i*) on semiempirical evaluation of the energy profile resulting from the progressive variation of the dihedral angle having as its central bond the 2,2′- or 3,3′- bisindole junction. The calculus is started from the global minimum of the analyzed structure in its initial *R* or *S* configuration (obtained by previous conformational search), and is terminated after that configuration underwent complete inversion;

(*ii*) on the structural optimization of both global minimum and transition state of the species involved in the analyzed enantiomerization process, whose difference in energy $\Delta E^{\#}$ affords a direct estimation of the enantiomerization barrier $\Delta G^{\#}$. In this way, therefore, by selection of a suitable level of theory, it was possible to assess, with expected good approximation, the $\Delta G^{\#}$ values with which the species **1b** and **4c** (which were not analyzed by experimental approach) should undergo enantiomerization at 25 °C.

It is important to stress the relevance that the here adopted theoretical approach can have in the perspective to be employed in the close future in designing structural changing of the configurationally instable 3,3′-biindole species, with the intent to significantly increase their stereochemical stability.

All experimental and computational results have been collected in Table 2, reporting, at the investigated temperatures, the related half-life times and, in cases in which it was possible

Table 2. Kinetic constants and activation parameters for the enantiomerization of **1a–b, 2a–b, 3, 4a–c** by theoretical (Semiempirical Energy Profile: SEP; Energy Difference between Transition and Fundamental States: $\Delta E^{\#}$), off-column enantioselective HPLC (eHPLC) and dynamic enantioselective HPLC (D-eHPLC) determinations.

Compound	Method	Solvent	*T* [°C]	k_{en} [s^{-1}]	$t_{0.5}$[a] [min]	$\Delta G^{\#}$ or $\Delta E^{\#}$ [kcal mol^{-1}]	$\Delta H^{\#}$ [kcal mol^{-1}]	$\Delta S^{\#}$ (entropy units, e.u.)
1a	Off-column (eHPLC)[b]	Ethyl acetate	60	1.687×10^{-7}	68493.7	29.90 ± 0.06		
	Theoretical (SEP)	Vacuum	25		1.10×10^{7}	29.7		
1b	Theoretical (SEP)	Vacuum	25		2.08×10^{12}	36.9		
2a	Off-column (eHPLC)[b]	Isooctane	70	9.77×10^{-6}	1183.0	28.05 ± 0.06		
			80	2.43×10^{-5}	237.5	28.24 ± 0.06	22.55 ± 0.5	−16.1 ± 1.0
			90	6.36×10^{-5}	90.8	28.37 ± 0.06		
2b	Off-column (eHPLC)[b]	Isooctane	90	1.2×10^{-6}	4821.6	31.24 ± 0.07		
3	On-column (D-eHPLC)[e]	n-Hexane-ethanol 100:0.5	15	1.04×10^{-4}	1.04×10^{-4}	22.10 ± 0.07		
			25	3.21×10^{-4}	3.21×10^{-4}	22.22 ± 0.07		
			30	4.27×10^{-4}	4.27×10^{-4}	22.43 ± 0.07	14.15 ± 2.0	−27.4 ± 6.5
			35	5.63×10^{-4}	5.63×10^{-4}	22.64 ± 0.07		
			40	8.66×10^{-4}	8.66×10^{-4}	22.75 ± 0.07		
	Theoretical (SEP)	Vacuum	25			22.7		
	Theoretical ($\Delta E^{\#}$)	Vacuum	25			22.3		
4a	On-column (D-eHPLC) [e]	n-Hexane-2-propanol-dichlomethane 100:1:5	25	7.51×10^{-5}	7.51×10^{-5}	23.08 ± 0.07		
			30	9.91×10^{-5}	9.91×10^{-5}	23.31 ± 0.07		
			35	1.83×10^{-4}	1.83×10^{-4}	23.33 ± 0.07	16.87 ± 3.4	−21.0 ± 11.2
			40	2.95×10^{-4}	2.95×10^{-4}	23.42 ± 0.07		
	Theoretical (SEP)	Vacuum	25			22.6		
	Theoretical ($\Delta E^{\#}$)	Vacuum	25			23.1		
4b	On-column (D-eHPLC) [e]	n-Hexane-2-propanol-dichlomethane 100:1:5	25	3.76×10^{-5}	3.76×10^{-5}	23.49 ± 0.07		
			30	6.12×10^{-5}	6.12×10^{-5}	23.60 ± 0.07		
			35	1.05×10^{-4}	1.05×10^{-4}	23.67 ± 0.07	16.34 ± 2.6	−23.9 ± 8.4
			40	1.41×10^{-4}	1.41×10^{-4}	23.88 ± 0.07		
			45	2.34×10^{-4}	2.34×10^{-4}	23.95 ± 0.07		
	Theoretical (SEP)	Vacuum	25			22.7		
4c	Theoretical (SEP)	Vacuum	25			22.6		
	Theoretical ($\Delta E^{\#}$)	Vacuum	25			22.8		

[a] Half-time for the racemization process; [b] Off-Column determination; [c] D-eHPLC conditions. Column: Chiralpak IB (250 mm × 4.6 mm I.D); eluent: n-hexane-ethanol-acetone 100:1:5 (v/v/v); flow rate: 1.0 mL/min; detector: UV at 280 nm; temperature: 25 °C; [d] D-eHPLC conditions. Column: Chiralpak IB-3 (250 mm × 4.6 mm I.D); eluent: n-hexane-ethanol 100:10 (v/v); flow rate: 1.0 mL/min; detector: UV at 380 nm; temperature: 25 °C; [e] D-eHPLC conditions. Column: Chiralpak IB-3 (250 mm × 4.6 mm I.D); eluent: n-hexane-ethanol 100:0.5 (v/v); flow rate: 2.0 mL/min; detector: UV at 310 nm; [f] D-eHPLC conditions. Column: Chiralpak IC (250 mm × 4.6 mm I.D); eluent: n-hexane-2-propanol-dichlomethane 100:1:5 (v/v/v); flow rate: 0.2 mL/min; detector: UV at 360 nm; [g] D-eHPLC conditions. Column: Chiralpak IC (250 mm × 4.6 mm I.D); eluent: n-hexane-2-propanol-dichlomethane 100:1:5 (v/v/v); flow rate: 0.2 mL/min; detector: UV at 254 nm. All $\Delta G^{\#}$ data were obtained by the relevant rate constant values through Eyring equation (transmission factor was set to 1).

to perform van't Hoff analysis, also the $\Delta H^{\#}$ and $\Delta S^{\#}$ contributions to $\Delta G^{\#}$.

By inspection of Table 2 data, it appears evident that the assessed $\Delta E^{\#}$ values for **1a**, **3**, **4a** and **4b** closely approach the experimental $\Delta G^{\#}$ ones, leaving therefore to expect acceptably good estimations for species **1b** and **4c** as well. It can also be stressed the reasonableness of the entropic contributions resulting from the van't Hoff analysis performed for the species **2a, 3, 4a** and **4b**, which range from −16.1 to −27.4 e.u.

These are, in fact, values perfectly compatible with the first order processes leading to the inversion of configuration investigated on the 2,2′- and 3,3′-biindole structures.

Comparatively looking at the $\Delta G^{\#}$ results for 2,2′-bindole monomers **1a, 1b, 2a, 2b** and 3,3′-biindole monomers **3, 4a–c**, the two families appear quite different in stereostability. In particular,

- the monomers with a 2,2′-biindole core should be considered *átropos*, *i.e.* configurationally stable in the considered temperature range, as it had been formerly pointed out for some of them.[5,6] In fact, between the peaks of the discriminated enantiomers was never visible an interposed plateau zone in the temperature range considered, so that to these species it was possible to apply the eHPLC off column racemization analysis approach, which resulted in all cases, also in agreement with theoretical computations, in $\Delta G^{\#}$ values significantly above the threshold value of 25 kcal mol^{-1}, and with estimated very long racemization times at room temperature;
- instead the monomers with 3,3′-biindole cores should be considered *trópos*, *i.e.* configurationally unstable, considering the shape of the enantioselective HPLC patterns (Figure 4), with increasing plateau formation between the enantiomer peaks as a function of a temperature increase. Consistently, the D-eHPLC was applied, resulting in estimated $\Delta G^{\#}$ values significantly below the 25 kcal mol^{-1} threshold, also in agreement with theoretical computations.

Such features are in good consistency with the CV observation of twin peak potential differences of an average of 0.16 V for the first family and of 0.38 V for the second family indicating that in the second case the interaction between the core moieties/equivalent redox centres is much stronger than in the first case, implying a much lower activation barrier. Interestingly, in the case of analogue couple **2a** *vs* **4a**, the difference in CV peak potential splitting is of 0.22 V, corresponding to an energy difference of about 5 kcal/mol, nearly coincident with the difference observed between the activation energy barriers of the two monomers. In other cases, differences are larger, but still with the order of magnitude of energy differences within some kcal/mol in both cases.

Instead, intriguingly, modulation from alkyl substituents resulted in different trends in CV experiments and in HPLC studies/ theoretical computations. In fact, as already mentioned, in CV larger potential differences were observed with hexyl chains with respect to methyl ones (**1b** *vs* **1a**, **2b** *vs* **2a**, **4b** *vs* **4a**), as in the case of higher reciprocal interaction between moieties, while in HPLC/computations higher energy barriers are estimated increasing the substituent length.

However, besides underlining that the contexts in which the effect of alkyl chains is evaluated are remarkably different (the CV case implying a solvent + supporting electrolyte system, respect to computational determinations in vacuum), an interesting clue should be considered, which we obtained analyzing by computational approach the geometries that the species **1a**, **1b**, **4a** and **4b** assume in the respective SEP calculations just before their change of configuration. More in particular, for each of these structures we took into consideration (i) the dihedral angle, ϕ, and ii) the bond order, **BO**, existing between the indole moieties. Values of ϕ close to zero should qualitatively indicate an acceptable good conjugation between the indoles, while **BO** greater than 1 give a quantitative indication of the established extent of conjugation. The results are: ϕ-**1a** = 14.1°, **BO-1a** = 1.022; ϕ-**1b** = 8.8°, **BO-1b** = 1.023; ϕ-**4a** = 38.4°, **BO-4a** = 1.027; ϕ-**4b** = 17.5°, **BO-4b** = 1.035. From their inspection a slightly better interaction clearly results between indole sites in **1b** with respect to **1a**, and in **4b** with respect to **4a**, just as pointed out by the respective ΔE° data. In other words, the structure deformation in the geometries of **1a**, **1b**, **4a** and **4b** close to their change of configuration principally involves the nearby periphery of the biindole nucleus, which, by contrast, as far as possible, tends to assume a coplanar arrangement to partially compensate the increase of energy of the whole structure.

Communication between Redox Centres in High-polarity Solvent Acetonitrile

Although in itself enantiomerization barriers do not depend on solvent polarity, not involving charged species, communication between redox centres at constant torsional barrier can be remarkably modulated by the solvent.[13,17] In particular, a polar solvent could attenuate it, resulting in partial charge shielding/ stabilization. As a consequence, if our assumption is right, working in acetonitrile instead of dichloromethane should result in narrower potential splitting in the biindole twin peak systems. This is indeed verified in our case, comparing CV patterns in CH_3CN (Figure 5; the Supporting Information also provides CV patterns for reductions, which can be observed in acetonitrile on account of the wider background) with the above discussed dichloromethane ones (Figure 3), as well as data in Table 3 with those for the same monomer in Table 1.

In the case of the 3,3′ monomers, the biindole core oxidations still result in twin systems of canonical reversible peaks (less canonical in the case **3** without phenyl spacer), but with significantly narrower $\Delta E^{\circ\prime}$splittings (0.23–0.29 V *vs* 0.31–0.42 V for 2,2′ systems) and a first peak located at more positive potentials ($E^{\circ\prime}$ = 0.34–0.35 V instead of 0.17–0.24 V ($Fc^{+}|Fc$)).

In the case of the 2,2′ monomers, featuring in dichloromethane a much narrower twin peak splitting respect to the 3,3′ series,

(*i*) in the absence of a phenyl spacer, a very narrow irreversible twin peak system (**1b**) or even a single irreversible peak (**1a**) is observed in acetonitrile, which however with

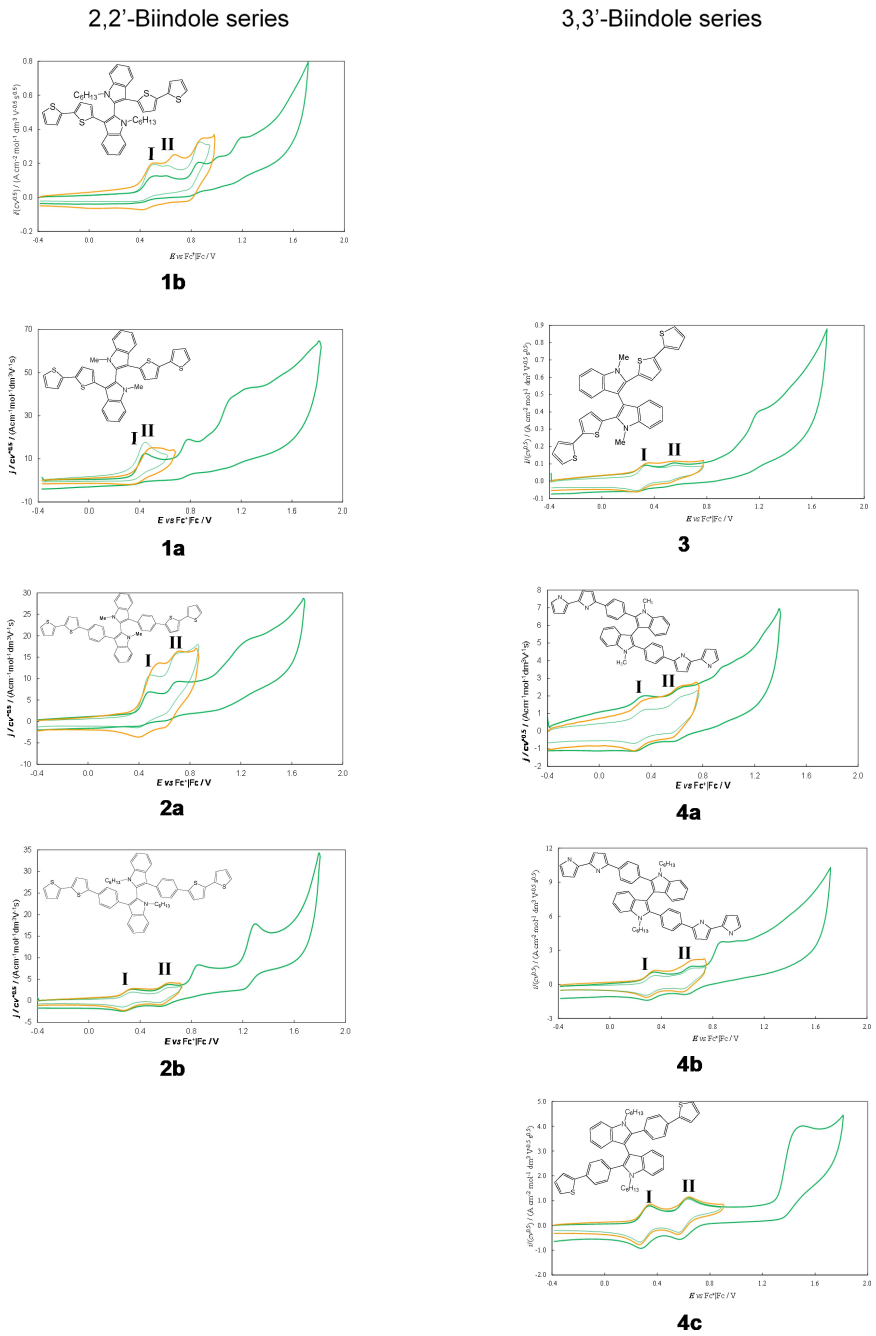

Figure 5. A synopsis of normalized 2,2′ (left) and 3,3′ (right) monomer CV patterns (concerning oxidations) in CH_3CN at 0.2 V/s (or 2 V/s, superimposed orange pattern)). Side by side are 2,2′ and 3,3′ analogue pairs.

increasing scan rates turn into twin systems of two nearly merging peaks of increasing reversibility;

(*ii*) in the presence of a phenyl spacer, a canonical twin peak system is observed, very similar to that obtained for the 3,3′ analogues.

In the case of monomer **1a**, the biindole CV pattern transition from two reversible peaks to a merging irreversible one was also clearly observed by progressively adding acetonitrile in the dichloromethane solution (Figure 6); the effect was much less evident in the **1b** case, in which some splitting at 0.2 V is observed also in acetonitrile. The wider available reduction potential window in acetonitrile also enables to observe the monomer reduction patterns, which mostly concern the (bi)thiophene wing systems, but still show some slightly splitting features.

Temperature Effect

All other conditions kept constant, communication between the redox centres across the torsional barrier should increase with

Table 3. Key features of the monomer CV patterns in CH_3CN at 0.2 V/s scan rate. (^{2}: at 2 V/s scan rate) . Potentials are expressed in volts and referred to $Fc^+|Fc$.

	E_{pI}	$E^{\circ\prime}_{I}$	E_{pII}	$E^{\circ\prime}_{II}$	$E_{pII}-E_{pI}$	$E^{\circ\prime}_{I}-E^{\circ\prime}_{II}$	E_{III}
2,2′-(N–Me)Ind_2T_4 (**1 a**)	0.44	0.39	n.d.		0.09		0.80,1.12
	0.49^2	0.43^2	0.58^2				
3,3′-(N–Me)Ind_2T_4 (**3**)	0.34	0.30	0.56	*0.53*	0.22	0.23	(1.03), 1.21
2,2′-(N-Hex)Ind_2T_4 (**1 b**)	0.51	0.46	0.62		0.11		0.87,1.03,1.15
	0.51^2	0.46^2	0.67^2		0.17		
2,2′-(N–Me)$Ind_2Ph_2T_4$ (**2 a**)	0.47	0.43	0.69		0.22		1.21
	0.51^2	0.45^2	0.71^2		0.20		
3,3′-(N–Me)$Ind_2Ph_2T_4$ (**4 a**)	0.35	0.31	0.62	0.59	0.27	0.28	0.94,1.25
2,2′-(N-Hex)$Ind_2Ph_2T_4$ (**2 b**)	0.35	0.30	0.61.	0.58	0.26	0.28	0.86, 1.31
3,3′-(N-Hex)$Ind_2Ph_2T_4$ (**4 b**)	0.35	0.32	0.64	0.62	0.29	0.29	0.82
3,3′-(N-Hex)$Ind_2Ph_2T_2$ (**4 c**)	0.34	0.31	0.63	0.60	0.29	0.29	1.45

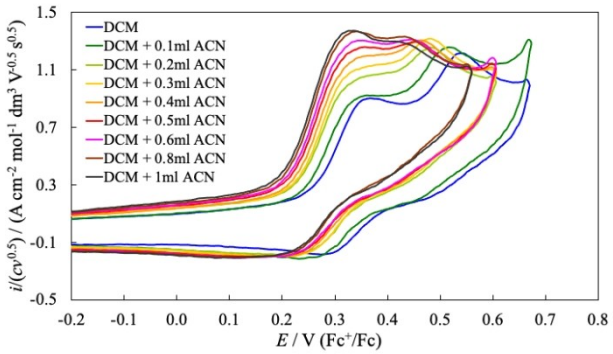

Figure 6. Modification of monomer **1 a** CV patterns starting from CH_2Cl_2 solvent (working volume ~3 cm^3) upon subsequent CH_3CN additions.

increasing temperature (and actually racemization half-times dramatically decrease with increasing temperature, Table 2).

This effect could be perceived in voltammetry experiments, too; in particular, it could be perceived in terms of increasing peak distance in the biindole cores with increasing temperature. Actually, such assumption looks in agreement with the observed trends of CV and DPV patterns of some 3,3′ monomers as a function of temperature (Figure 7).

In fact, although the twin peaks appear to maintain reversible features, their twin peak reciprocal distances $\Delta E^{\circ\prime}$ appear to increase with temperature; in particular, such trends can be rationalized in terms of linear $\Delta E^{\circ\prime}$ *vs* $1/T$ linear relationships (Figure 8). Notably, the temperature effect enhancing the interaction between redox centres looks much more remarkable in the experiments carried out in polar solvent CH_3CN, in which interaction between the redox centres would be intrinsically more difficult.

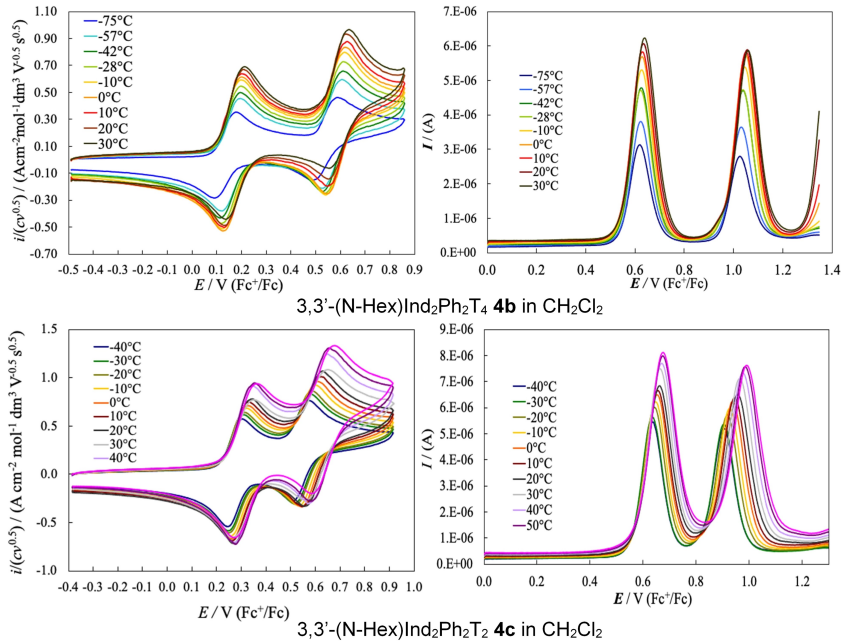

Figure 7. Temperature effect on the CV and DPV patterns of some 3,3′ biindole monomers.

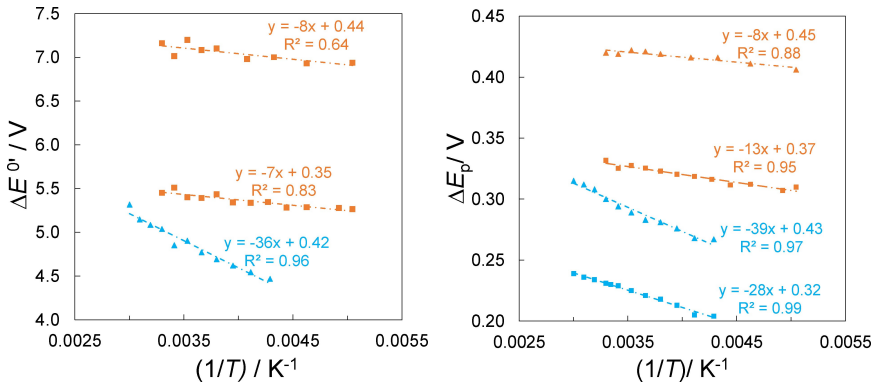

Figure 8. Temperature effect on the $\Delta E^{\circ\prime}$ twin peak splitting of some 3,3′ biindole monomers. Left: data from CVs. Right: data from DPVs; orange: CH_2Cl_2, blue: CH_3CN.

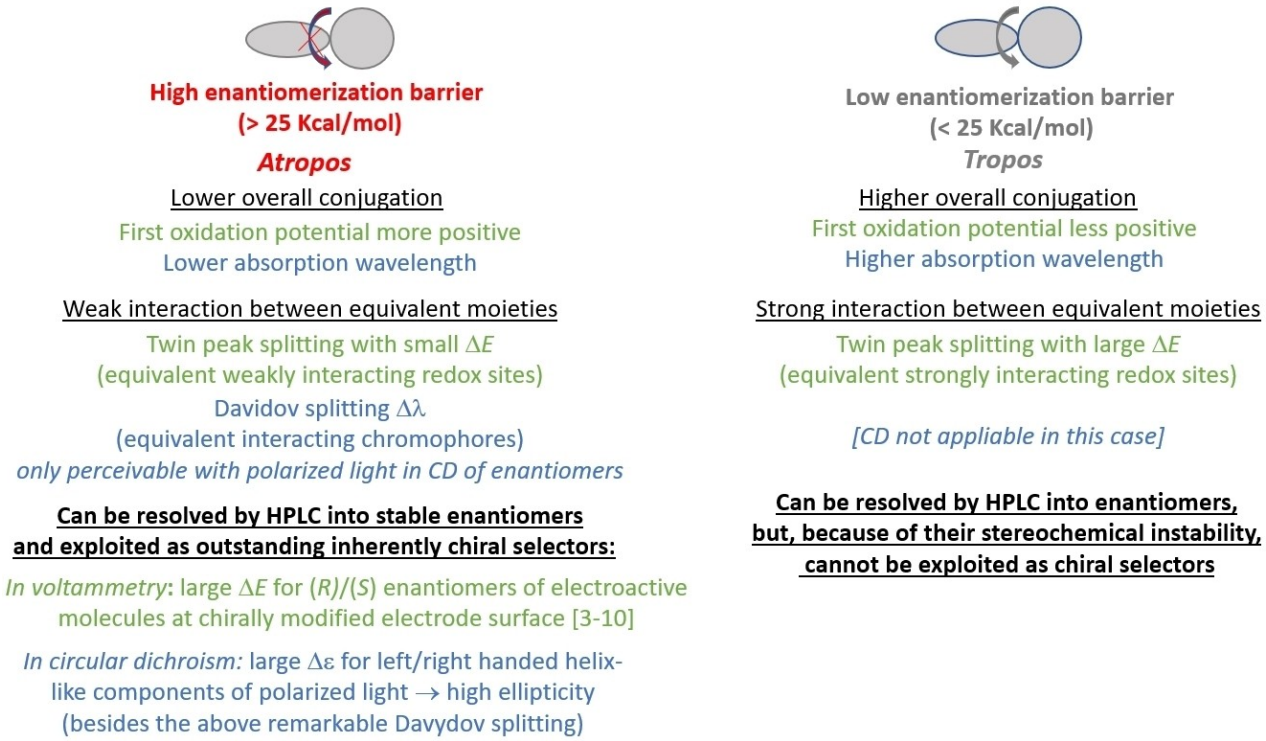

Figure 9. A summary of features and implications in voltammetry (green) and UV-Vis spectroscopy (blue) of *atropos vs tropos* systems.

Conclusion

With molecules consisting of two equivalent redox centres reciprocally interacting through a torsional barrier, like the 2,2′- and 3,3′-biindole monomer analogues here discussed as model cases, the twin peak potential splitting observed in voltammetry for the first oxidation of the biheteroaromatic core nicely accounts for the energy barrier height and relevance. In particular, the lower the barrier, the larger the peak potential splitting, with modulation by solvent and temperature. Specifically, working in a solvent of higher polarity results in smaller peak splitting, consistent with weaker interactions, as in other cases of interacting redox centres; on the other hand, increasing temperature results in increasing potential splitting, pointing to decreasing barrier relevance.

As summarized in Figure 9, the height of the energy barrier is a determining factor for the electrochemical and spectroscopic features of the monomers as well as for their configurational stability and applicability for enantioselection purposes. For example, in our study case, the 3,3′ monomers, featuring very large twin peak splittings in CV, are "*tropos*" systems having a low torsional barrier, so that they cannot exist as stable enantiomers at room temperature. Instead their 2,2′ analogues, featuring much smaller twin peak splittings in CV, are "*atropos*" systems which can be separated by enantioselective HPLC into stable enantiomers. The latter ones provide powerful "inherently chiral" selectors which display outstanding

enantioselection properties in chiral electroanalysis and electrochemistry as well as in chiroptical spectroscopy, with fascinating reciprocal correlations.

Experimental Section

Monomer Synthesis

General Information

All reactions were performed with oven dried laboratory glassware, under nitrogen atmosphere unless otherwise indicated. All reactants and dry solvent were purchased from Sigma Aldrich, Tokyo Chemical Industry and Fluorochem and used as received. TLC analysis were performed on ALUGRAM® Xtra SIL G/UV254 (0.2 mm thin layer depth; Macherey-Nagel). Gravimetric chromatography columns were performed using silica gel (particles diameter: 0.63–2.00 mm) as stationary phase. ^{1}H-NMR spectra were recorded with Bruker AVANCE instrument operating at 400.13 MHz with TMS as internal standard. ^{13}C-NMR spectra were recorded at 100.56 MHz with total proton decoupling with TMS as internal standard. Mass analyses were performed by using a VG 7070 EQ-HF instrument. Moreover, accurate masses (reported in the SI) were obtained for six monomers with a Synapt G2-Si QTof mass spectrometer - ZsprayTM ESI-probe for electrospray ionization (Waters). IR spectra were recorded with a FT-IR Thermo Scientific Nicolet iS10 Smart iTR. Melting points were obtained with a Gallenkamp instrument.

Synthesis of 3,3′-Di-2,2′-bithien-5-yl-1,1′-dihexyl-1*H*,1′*H*-2,2′-biindole (1 b). KOH (280 mg, 5.0 mmol) was added to a stirred solution of **6**[5] (560 mg, 1.0 mmol) in DMF (6 mL), at 0 °C. After 15 min 1-bromohexane (1.65 g, 10.0 mmol) was added dropwise, the mixture was then allowed to warm to r.t. and left under stirring for 36 h. H_2O (50 mL) and CH_2Cl_2 (30 mL) were added, the organic layer was separated and the aqueous phase was extracted with CH_2Cl_2 (3× 20 mL). The collected organic layers were dried (Na_2SO_4) and the solvent was removed under reduced pressure. MeOH (10 mL) was added to the residue, the precipitate was filtered, washed with H_2O and dried in vacuum to afford **1 b** (605 mg, 83%). M.p. 135 °C; ^{1}H NMR (300 MHz, $CDCl_3$) δ 8.21 (d, J=7.5 Hz, 2H), 7.46–7.31 (m, 6H), 7.14 (d, J=4.8 Hz, 2H), 7.04 (d, J=3.6 Hz, 2H), 7.00–6.94 (m, 4H), 6.82 (d, J=3.6 Hz, 2H), 3.92–3.68 (m, 4H), 1.62–1.46 (m, 2H), 1.38–1.20 (m, 2H), 1.19–1.00 (m, 12H), 0.72 (t, J=7.0 Hz, 6H);^{13}C NMR (75 MHz, $CDCl_3$) δ 137.7, 137.0, 136.0, 135.3, 127.7, 126.6, 125.8, 124.5, 124.2, 123.8, 123.2, 123.2, 120.7, 120.6, 113.3, 110.6, 44.6, 31.4, 29.7, 26.7, 22.4, 13.9; MS (EI): m/z=728 $[M]^+$.

Synthesis of 2,2′-Di-2,2′-bithien-5-yl-1,1′-dimethyl-1*H*,1′*H*-3,3′-biindole (3). 2,2′-Bithiophene-5-carboxaldehyde (455 mg, 2.4 mmol) and a few drops of a 37% HCl aqueous solution were added to a solution of alkyne **8** (120 mg, 0.58 mmol) in MeCN (8 mL). The reaction mixture was refluxed for 5 h, then the solvent was removed under reduced pressure. The residue was dissolved in CH_2Cl_2 and washed with a saturated sodium bicarbonate aqueous solution. The organic phase wasdried over $MgSO_4$, filtered and solvent removed under reduced pressure. The residue including the 2,2′-di([2,2′-bithiophen]-5-yl)-1H,1′H-3,3′-biindole was used without any further purification for next step. The crude product was dissolved in DMF (5 mL) and then KOH (86 mg, 1.52 mmol) was added at r.t. The reaction mixture was stirred for 0.5 h, then iodomethane (270 mg, 1.9 mmol) was added and the solution stirred for 48 h. After removal of the solvent under reduced pressure, the product was purified by gravimetric column chromatography (*n*-hexane/EtOAc 8:2) to afford compound **3** (98 mg, 29%) as a yellow solid. ^{1}H NMR (400 MHz, $CDCl_3$) δ 7.48 (d, J=7.9 Hz, 2H), 7.40 (d, J=8.2 Hz, 2H), 7.30 (d, J=8 Hz, 2H), 7.17 (d, J=5.0 Hz, 2H), 7.11 (t, J=7.3 Hz, 2H), 6.96 (ddd, J=14.3, 9.0, 3.1 Hz, 6H), 6.52 (d, J=3.7 Hz, 2H), 3.81 (s, 6H). ^{13}C NMR (100 MHz, $CDCl_3$) δ: 138.9, 137.8, 138.3, 131.6, 131.2, 129.1, 128.8, 127.8, 124.2, 123.6, 123.5, 122.3, 120.8, 119.7, 109.4, 109.3, 31.2. MS (ESI): 588 (100%).

Synthesis of Compounds 11 a,b: General Procedure. A solution of dibromoderivative **10** (542 mg, 1 mmol) and KOH (280 mg, 5 mmol) in DMF (10 mL), was stirred for 0.5 h, then the suitable haloderivative (10 mmol) was added and the mixture stirred for 48 h. The solvent was removed under reduced pressure and the residue was purified by gravimetric column chromatography (*n*-hexane/EtOAc 8:2).

2,2′-Bis(4-bromophenyl)-1,1′-dimethyl-1*H*,1′*H*-3,3′-biindole (11 a). MeI was used as alkylating agent; yield 72%; m.p. 265 °C; ^{1}H NMR (400 MHz, DMSO-d_6) δ 7.52 (d, J=8.3 Hz, 1H), 7.36 (d, J=8.5 Hz, 2H), 7.26–7.13 (m, 2H), 6.99 (t, J=7.4 Hz, 1H), 6.84 (d, J=8.5 Hz, 2H), 3.62 (s, 3H). ^{13}C NMR (101 MHz, DMSO-d_6) δ 137.8, 137.3, 132.2, 131.4, 131.2, 128.2, 122.2, 121.3, 120.1, 119.9, 110.7, 107.1, 31.5; MS (EI): m/z=570 $[M]^+$.

2,2′-Bis(4-bromophenyl)-1,1′-dihexyl-1H,1′H-3,3′-biindole (11 b). 1-Bromohexane was used as alkylating reagent; yield 93%.; m.p.: 127 °C

^{1}H NMR (400 MHz, $CDCl_3$) δ: 7.57 (d, J=7.8 Hz, 2H), 7.43 (d, J=8.2 Hz, 2H), 7.30 (t, J=7.6 Hz, 2H), 7.20 (d, J=8.4 Hz, 4H), 7.14 (t, J=7.4 Hz, 2H), 6.55 (d, J=8.4 Hz, 4H), 4.08–3.94 (m, 4H), 1.77–0.99 (m, 16H), 0.79 (t, J=7.0 Hz, 6H). ^{13}C NMR (100 MHz, $CDCl_3$) δ: 137.0, 137.0, 131.6, 131.4, 131.0, 129.1, 121.8, 121.1, 121.0, 119.4, 110.0, 107.9, 44.0, 31.2, 29.7, 26.3, 22.4, 13.9. MS (EI): m/z=708 $[M]^+$.

Synthesis of Compounds 4 a,b,c: General Procedure.–(4,4,5,5)-Tetramethyl-1,3,2-dioxaborolan-2-yl)-2,2′-bithiophene or 2-thienylboronic acid (6.1 mmol), $Pd(PPh_3)_4$ (380 mg, 0.33 mmol) and potassium carbonate (3 g, 21.7 mmol) were added to a solution of the dibromoderivative **11 a** or **11 b** (2.2 mmol) in THF (150 mL) and water (15 mL). The reaction mixture was refluxed for 20 h and the solvent removed under reduced pressure. The residue was dissolved in DCM and washed with water; the organic phase was dried over $MgSO_4$ and dried under reduced pressure. Crude product was purified by gravimetric column chromatography (CH_2Cl_2/*n*-hexane 1:9).

2,2′-Bis[4-(2,2′-bithien-5-yl)phenyl]-1,1′-dimethyl-1*H*,1′*H*-3,3′-biindole (4 a). Yield 59%; m.p. >275 °C. ^{1}H-NMR (400 MHz, DMSO-d_6): δ 7.56–7.53 (m, 2H), 7.48–7.43 (m, 2H), 7.36–7.33 (m, 2H), 7.25 (t, 1H, J=8 Hz), 7.21 (t, 1H, J=8 Hz), 7.12 (t, 1H, J=8 Hz), 7.01 (m, 1H), 6.96 (d, 2H, J=8 Hz), 6.86 (d, 1H, J=8 Hz), 3.67 (s, 3H). We weren't able to record the ^{13}C NMR spectrum due to the low solubility of the compound.

2,2′-Bis[4-(2,2′-bithien-5-yl)phenyl]-1,1′-dihexyl-1*H*,1′*H*-3,3′-biindole (4 b). Yield 75%. ^{1}H NMR (400 MHz, DMSO-d_6) δ: ^{1}H NMR (400 MHz, DMSO-d_6) δ 7.58–7.51 (m, 4H), 7.45 (dd, J=8.2, 6.1 Hz, 6H), 7.36–7.31 (m, 4H), 7.25–7.15 (m, 4H), 7.11 (dd, J=5.1, 3.6 Hz, 2H), 6.99 (t, J=7.2 Hz, 2H), 6.91 (d, J=8.4 Hz, 4H), 4.21–4.07 (m, 4H), 1.58–1.41 (m, 4H), 1.09–0.88 (m, 12H), 0.65 (t, J=7.0 Hz, 6H). ^{13}C NMR (101 MHz, DMSO-d_6) δ: 142.1, 138.3, 137.1, 136.8, 136.5, 132.4, 131.8, 130.7, 129.1, 128.9, 126.1, 125.7, 125.3, 125.2, 124.6, 122.1, 120.1, 119.8, 111.0, 107.7, 43.6, 31.0, 29.5, 25.9, 22.3, 14.1. MS (EI) 881 (100%).

1,1′-Dimethyl-2,2′-bis[4-(2-thienyl)phenyl]-1H,1′H-3,3′-biindole (4 c). Yield 97%). ^{1}H NMR (400 MHz, $CDCl_3$) δ 7.64 (d, J=7.8 Hz, 2H), 7.44 (d, J=8.2 Hz, 2H), 7.34–7.26 (m, 10H), 7.19–7.10 (m, 4H), 6.72–6.65 (m, 4H), 4.05 (t, J=7.6 Hz, 4H), 1.77–1.47 (m, 4H), 1.24–0.99 (m,

12H), 0.76 (t, $J=6.9$ Hz, 6H); ^{13}C NMR (101 MHz, $CDCl_3$) δ 144.5, 137.9, 137.0, 132.5, 131.7, 130.5, 129.3, 128.1, 125.3, 124.8, 122.9, 121.5, 121.0, 119.2, 109.9, 107.9, 44.0, 31.2, 29.8, 26.4, 22.4, 13.9.

Enantioselective HPLC

HPLC enantioseparations of **1a**, **2a**, **2b**, **3**, **4a** and **4b** were performed by using stainless-steel Chiralpak IB (250 mm×4.6 mm and 250 mm×10 mm) columns (Chiral Technologies Europe, Illkirch-Graffenstaden, France). All HPLC solvents were purchased from Sigma-Aldrich (Milan, Italy) and used without further purification. The analytical HPLC apparatus consisted of a pump equipped with a Rheodyne injector, a 20 μL sample loop, a HPLC oven, and a UV/CD detector. For semipreparative separations, a 1000 μL sample loop was used.

Off-column configuration stability study. In the off-column racemization study, a solution of the more retained enantiomer of **1a** (or **2a**) (concentration about 0.1 mg mL^{-1}) was held at a fixed temperature in a closed vessel. The temperature was monitored by using a Julabo thermostat. Samples were withdrawn at recorded time intervals and analyzed by HPLC on the Chiralpak IB (250 mm× 4.6 mm) column under the analytical conditions reported in Table 2.

Simulation of Dynamic Chromatograms

Simulations of dynamic chromatograms were performed with the Auto-DHPLC-y2k lab-made computer program, which implements both stochastic and theoretical plate models[46–56] and is able to take into account all types of first-order interconversion, as well as tailing effects. In the present study, simulations of dynamic chromatograms of 3,3′-biindole derivatives were carried out with stochastic model, also taken into consideration tailing effects and driving the optimization in automatic fashion by minimizing the RMS of the differences existing -between experimental and simulated chromatogram profiles.

Molecular Modeling Calculations

All calculations were performed with the software package SPARTAN 10, v. 1.1.0 (Wavefunction, Irvine, CA). Global Minima Energy conformations of all the 2,2′–3,3′-biindole derivatives studied in the present work (GMn, with n denoting the particular biindole species) have been obtained at the semiempirical AM1 level of theory by the conformational search algorithm implemented in Spartan. For the species **1a**, **1b**, **4a** and **4b** the bond order of the bond connecting the indole cycles was computed at the semiempirical AM1 level of theory. Starting from these GMn conformations, for the species **1a**, **1b**, **3**, **4a**, **4b**, **5** they were computed the relevant Energy Profiles at the semiempirical AM1 level of theory by progressive rotation around the bond responsible for the 3–3′-bisindole junction, according to the related algorithm implemented in Spartan. Structures of ground and transition states of compounds 3, 4a, 4b and 5 (GS_x and TS_x, respectively, with x denoting the species), required for the calculation of the $\Delta E^{\#}_x = TS_x - GS_x$ differences that afford the direct estimation of the enantiomerization barriers $\Delta G^{\#}_x$ of the 3,3′-biindole derivatives, were next obtained starting from the respective GMn conformations and from the geometries characterized by the higher energy value just found from the above quoted semiempirical energy profiles of the considered species, respectively. In a first step these were optimized at the HF/3 21G level of theory (all the TS_x geometries were also validated as saddle points by checking the presence among the computed vibrational modes of only one imaginary frequency). Next, all the so minimized structures were submitted to single point energy calculations at the M062X/6-31+G*level of theory.

Electrochemical Characterization of the Monomers

The inherently chiral monomers in 0.0005 M concentration were analyzed by CV experiments (in the 0.05–2 V s^{-1} scan rate range) in a glass mini cell (3 cm^3 of solution), with glassy carbon (GC, 0.033 cm^2) as working electrode, a platinum wire as counter and a saturated calomel as reference electrode, inserted in a double jacket. Monomers were dissolved in ACN or CH_2Cl_2 with $TBAPF_6$ 0.1 M as supporting electrolyte and the potential values were referred to the $Fc^+|Fc$ intersolvental reference redox couple (~ 0.39 V for ACN and ~0.49 V for CH_2Cl_2).

Differential Pulse Voltammetry (DPV) to Study the Racemization Barrier

Monomers in 0.0005 M concentration were dissolved in ACN or CH_2Cl_2 with $TBAPF_6$ 0.1 M as supporting electrolyte. Measurements were carried out in a minicell with a glassy carbon tip used as working electrode together with a Pt disk as a counter and an aqueous saturated calomel asa reference electrode inserted into a double jacket with a porous frit to avoid water and chloride leakage. The glass minicell was immersed in a thermostatic bath where dry ice was mixed with methanol to reach very low temperatures (monitored by means of a mercury thermometer). Differential pulse voltammetric responses were measured every 5–10 °C in order to reveal any changes in the distance between the two first monomer anodic peaks.

Acknowledgements

Fondazione Cariplo and Regione Lombardia as well as Università degli Studi di Milano are acknowledged for support to the research group in Milano. Fondazione Cariplo and Università degli Studi dell'Insubria are acknowledged for support to the research group in Como. The accurate mass determinations were performed at the Unitech Technological Platform at Università degli Studi di Milano, care of Dr. Marco Pappini and Dr. Milda Stuknytė. Ms. Rossella Monaco is also acknowledged for some preliminary CV experiments. Open Access Funding provided by Universita degli Studi di Milano within the CRUI-CARE Agreement.

Conflict of Interest

The authors declare no conflict of interest.

Keywords: Voltammetry · interacting equivalent redox centres/chromophores · torsional barrier · enantioselective HPLC · configurational stability

[1] S. Arnaboldi, S. Grecchi, M. Magni, P. Mussini, *Curr. Opin. Electrochem.* **2018**, *7*, 188–199.

[2] S. Arnaboldi, S. Cauteruccio, S. Grecchi, T. Benincori, M. Marcaccio, A. Orbelli Biroli, G. Longhi, E. Licandro, P. R. Mussini, *Chem. Sci.* **2019**, *10*, 1539–1548.
[3] F. Sannicolò, S. Arnaboldi, T. Benincori, V. Bonometti, R. Cirilli, L. Dunsch, W. Kutner, G. Longhi, P. R. Mussini, M. Panigati, M. Pierini, S. Rizzo, *Angew. Chem. Int. Ed.* **2014**, *53*, 2623–2627; *Angew. Chem.* **2014**, *126*, 2661–2665.
[4] F. Sannicolò, P. R. Mussini, T. Benincori, R. Martinazzo, S. Arnaboldi, G. Appoloni, M. Panigati, E. Quartapelle Procopio, V. Marino, R. Cirilli, S. Casolo, W. Kutner, K. Noworyta, A. Pietrzyk-Le, Z. Iskierko, K. Bartold, *Chem. Eur. J.* **2016**, *22*, 10839–10847.
[5] S. Arnaboldi, T. Benincori, A. Penoni, L. Vaghi, R. Cirilli, S. Abbate, G. Longhi, G. Mazzeo, S. Grecchi, M. Panigati, P. R. Mussini, *Chem. Sci.* **2019**, *10*, 2708–2717.
[6] L. Scapinello, S. Grecchi, S. Rossi, F. Arduini, S. Arnaboldi, A. Penoni, R. Cirilli, P. R. Mussini, T. Benincori, *Chem. Eur. J.* **2021**, *27*, 13190–13202.
[7] C. Malacrida, L. Scapinello, R. Cirilli, S. Grecchi, A. Penoni, T. Benincori, S. Ludwigs, *ChemElectroChem.* **2021**, *8*, 3250–3261.
[8] G. Bonetti, S. Arnaboldi, S. Grecchi, G. Appoloni, E. Massolo, S. Rossi, R. Martinazzo, F. Orsini, P. R. Mussini, T. Benincori, *Molecules* **2020**, *25*, 2175.
[9] S. Arnaboldi, T. Benincori, R. Cirilli, W. Kutner, M. Magni, P. R. Mussini, K. Noworyta, F. Sannicolò, *Chem. Sci.* **2015**, *6*, 1706–1711.
[10] S. Arnaboldi, T. Benincori, R. Cirilli, S. Grecchi, L. Santagostini, F. Sannicolò, P. R. Mussini, *Anal. Bioanal. Chem.* **2016**, *408*, 7243–7254.
[11] C. Fraschetti, M. Pierini, C. Villani, F. Gasparrini, S. Levi Mortera, A. Filippi, M. Speranza, *Chem. Eur. J.* **2011**, *17*, 3078–3081.
[12] G. K. E. Scriba, *Chromatographia* **2012**, *75*, 815–838.
[13] T. Eralp, A. Ievins, A. Shavorskiy, S. J. Jenkins, G. Held, *J. Am. Chem. Soc.* **2012**, *134*, 9615–9621.
[14] M. Chojecki, D. Rutkowska-Zbik, T. Korona, *Phys. Chem. Chem. Phys.* **2019**, *21*, 22491–22510.
[15] A. J. Bard, L. R. Faulkner, *Electrochemical Methods. Fundamental and Applications*, 2nd edition, Wiley, Hoboken, NJ, USA **2000**.
[16] R. F. Winter, *Organometallics* **2014**, *33*, 4517–4536.
[17] K. Lam, W. E. Geiger, *Influence of Molecular and Medium Effects on Two-Electron Processes, Chapter 11, in O. Hammerich, B. Speiser* (Eds.) *Organic Electrochemistry,* 5th edition revised and expanded, CRC Press/Taylor & Francis, Boca Raton/London/New York, **2016**.
[18] J.-M. Savéant, *Elements of Molecular and Biomolecular Electrochemistry. An Electrochemical Approach to Electron Transfer Chemistry*, Wiley, Hoboken, NJ, USA, **2006**.
[19] D. Miesel, A. Hildebrandt, H. Lang, *Curr. Opin. Electrochem.* **2018**, *8*, 39–44.
[20] A. Liska, J. Ludvik, *Curr. Opin. Electrochem.* **2018**, *8*, 45–51.
[21] S. Santi, A. Bisello, R. Cardena, A. Donoli, *Dalton Trans.* **2015**,*44*, 5234–5257.
[22] Y. Wu, J.-M. Han, M. Hong, M. D. Krzyaniak, A. K. Blackburn, I. R. Fernando, D. D. Cao, M. R. Wasielewski, J. Fraser Stoddart, *J. Am. Chem. Soc.* **2018**, *140*, 515–523.
[23] H. F. Bettinger, R. Einholz, A. Göttler, M. Junge, M.-S. Sättele, A. Schnepf, C. Schrenk, S. Schundelmeier, B. Speiser, *Org. Chem. Front.* **2017**, *4*, 853–860.
[24] M. López-Tenés, C. Serna, M. M. Moreno, Á. Molina, *Electrochim. Acta* **2007**, *25*, 103–118.
[25] K. Aoki, J. Chen, H. Nishihara, T. Hirao, *J. Electroanal. Chem.* **1996**, *416*, 151–155.
[26] K. Ventura, M. B. Smith, J. R. Prat, L. E. Echegoyen, D. Villagrán, *J. Chem. Educ.* **2017**, *94*, 526–529.
[27] M. Parthey, M. Kaupp, *Chem. Soc. Rev.* **2014**, *43*, 5067–5088.
[28] C. Lambert, G. Nöll, *Angew. Chem. Int. Ed.* **1998**, 37, 2108–2110.
[29] M. Heitzmann, J.-C. Moutet, J. Pécaut, O. Reynes, G. Royal, E. Saint-Aman, G. Serratrice, *Eur. J. Inorg. Chem.* **2003**, *20*, 3767–3773.
[30] A. Bossi, L. Falciola, C. Graiff, S. Maiorana, C. Rigamonti, A. Tiripicchio, E. Licandro, P. R. Mussini, *Electrochim. Acta* **2009**, *54*, 5083–5097.
[31] C. Baldoli, E. Licandro, S. Maiorana, D. Resemini, C. Rigamonti, L. Falciola, M. Longhi, P. R. Mussini, *J. Electroanal. Chem.* **2005**, *585*, 197–205.
[32] M. Parthey, M. Kaupp, *Chem. Soc. Rev.* **2014**, *43*, 5067–5088.
[33] J. T. Vázquez, *Tetrahedron: Asymmetry* **2017**, 28, 1199–1211.
[34] N. Berova, L. Di Bari, G. Pescitelli, *Chem. Soc. Rev.* **2007**, *36*, 914–931.
[35] R. C. Larock, E. K. Yum, *J. Am. Chem. Soc.* **1991**, *113*, 6689–6690.
[36] R. C. Larock, E. K. Yum, M. D. Refvik, *J. Org. Chem.* **1998**, *63*, 7652–7662.
[37] G. Abbiati, A. Arcadi, E. Beccalli, G. Bianchi, F. Marinelli, E. Rossi, *Tetrahedron* **2006**, *62*, 3033–3039.
[38] M. G. Saulnier, D. B. Frennesson, M. S. Deshpande, D. M. Vyas, *Tetrahedron Lett.* **1995**, *36*, 7841–7844.
[39] C. I. Lin, S. Selvi, J. M. Fang, P. T. Chou, C. H. Lai, Y. M. Cheng, *J. Org. Chem.* **2007**, *72*, 3537–3542.
[40] W. Lee, N. Cho, J. Kwon, J. Ko, J. I. Hong, *Chem. Asian J.* **2012**, *7*, 343–350.
[41] C. P. Tüllmann, Y. Chen, R. J. Schuster, P. Knochel, *Org. Lett.* **2018**, *20*, 1–50.
[42] Z. Wu, Z. An, X. Chen, P. Chen, *Org. Lett.* **2013**, *15*, 1456–1459.
[43] A. Arcadi, M. Chiarini, G. D'Anniballe, F. Marinelli, E. Pietropaolo, *Org. Lett.* **2014**, *16*, 1736–1739.
[44] T. Niu, Y. Zhang, *Tetrahedron Lett.* **2010**, *51*, 6847–6851.
[45] J. Heinze, B. A. Frontana-Uribe, S. Ludwigs, *Chem. Rev.* **2010**, *110*, 4724–4771.
[46] I. Noviandri, K. N. Brown, D. S. Fleming, P. T. Gulyas, P. A. Lay, A. F. Masters, L. Phillips, *J. Phys. Chem. B* **1999**, *103*, 6713–6722.
[47] A. Rosetti, G. Bonetti, C. Villani, T. Benincori, R. Cirilli, *Chirality* **2021**, *33*, 146–152.
[48] F. Gasparrini, L. Lunazzi, A. Mazzanti, M. Pierini, K. M. Pietrusiewicz, C. Villani, *J. Am. Chem. Soc.* **2000**, *122*, 4776.
[49] F. Gasparrini, I. D'Acquarica, M. Pierini, C. Villani, *J. Sep. Sci.* **2001**, *24*, 941.
[50] C. Dell'Erba, F. Gasparrini, S. Grilli, L. Lunazzi, A. Mazzanti, M. Novi, M. Pierini, C. Tavani, C. Villani, *J. Org. Chem.* **2002**, *67*, 1663.
[51] F. Gasparrini, S. Grilli, R. Leardini, L. Lunazzi, A. Mazzanti, D. Nanni, M. Pierini, M. Pinamonti, *J. Org. Chem.* **2002**, *67*, 3089.
[52] A. Dalla Cort, F. Gasparrini, L. Lunazzi, L. Mandolini, A. Mazzanti, C. Pasquini, M. Pierini, R. Rompietti, L. Schiaffino, *J. Org. Chem.* **2005**, *70*, 8877.
[53] A. Ciogli, A. Dalla Cort, F. Gasparrini, L. Lunazzi, L. Mandolini, A. Mazzanti, C. Pasquini, M. Pierini, L. Schiaffino, F. Yafteh Mihan, *J. Org. Chem.* **2008**, *73*, 6108.
[54] R. Cirilli, R. Ferretti, F. La Torre, D. Secci, A. Bolasco, S. Carradori, M. Pierini, *J. Chromatogr. A* **2007**, *1172*, 160.
[55] R. Cirilli, R. Costi, R. Di Santo, F. La Torre, M. Pierini, G. Siani, *Anal. Chem.* **2009**, *81*, 3560.
[56] R. Cirilli, R. Costi, R. Di Santo, F. Gasparrini, F. La Torre, M. Pierini, G. Siani, *Chirality* **2009**, *21*, 24.
[57] M. Jung, *QCPE Bull.* **1992**, *12*, 52.
[58] O. Trapp, V. Schurig, *Comput. Chem.* **2001**, *25*, 187.
[59] T. Benincori, V. Bonometti, R. Cirilli, P. R. Mussini, A. Marchesi, M. Pierini, T. Pilati, S. Rizzo, F. Sannicolò, *Chem. Eur. J.* **2013**, *19*, 165–181.
[60] S. Rizzo, T. Benincori, V. Bonometti, R. Cirilli, P. R. Mussini, M. Pierini, T. Pilati, F. Sannicolò, *Chem. Eur. J.* **2013**, *19*, 182–194.
[61] R. Cirilli, R. Costi, R. Di Santo, F. La Torre, M. Pierini, G. Siani, *Anal. Chem.* **2009**, *81* (9), 3560–3570.
[62] D. Rotili, A. Samuele, D. Tarantino, R. Ragno, I. Musmuca, F. Ballante, G. Botta, L. Morera, M. Pierini, R. Cirilli, M. B. Nawrozkij, E. Gonzalez, B. Clotet, M. Artico, J. A. Esté, G. Maga, A. Mai, *J. Med. Chem.* **2012**, *55*, 3558–3562.
[63] S. Rizzo, S. Arnaboldi, V. Mihali, R. Cirilli, A. Forni, A. Gennaro, A. A. Isse, M. Pierini, P. R. Mussini, F. Sannicolò, *Angew. Chem. Int. Ed.* **2017**, *56*, 1–5; *Angew. Chem.* **2017**, *129*, 1–1.

Manuscript received: July 2, 2021
Revised manuscript received: October 5, 2021
Accepted manuscript online: October 20, 2021